Available online at www.sciencedirect.com
SCIENCE DIRECT®
ELSEVIER
International Journal of Solids and Structures 43 (2006) 2364–2377
INTERNATIONAL JOURNAL OF SOLIDS and STRUCTURES
www.elsevier.com/locate/ijsolstr

Experimental and numerical investigations of the deformation of soft materials under tangential loading

X.J. Ren [a,*], C.W. Smith [b], K.E. Evans [b], P.J. Dooling [c], A. Burgess [c], J. Wiechers [d], N. Zahlan [c]

[a] *School of Engineering, Liverpool John Moores University, Liverpool L3 3AF, UK*
[b] *School of Engineering, University of Exeter, Exeter EX4 4QF, UK*
[c] *ICI Strategic Technology Group, Wilton, UK*
[d] *Uniqema R&D, Gouda, The Netherlands*

Received 7 January 2005; received in revised form 23 May 2005
Available online 10 October 2005

Abstract

The surface 'tensile test', in which tangential loads are applied through surface mounted adhesive tapes, is a viable method for the assessment of mechanical properties of soft materials, particularly biological soft materials in vivo. In the present work the deformation pattern and force–displacement relationship in the surface tensile test were experimentally investigated using surface displacement analysis (SDA) and numerically simulated using finite element modelling. The experimental and FE results showed close agreement using silicone rubber as a model material. The force–displacement relationship was found to be dependent on the tape separations. SDA measurements and FE simulation showed that the displacement and strain fields were not uniform and the distribution pattern varies with tape separation. A combined experimental–numerical approach to inversely extract material properties using multiple tests with different length scales is proposed and assessed using a model material.

Keywords: Tangential loading; Inverse engineering; Soft materials

1. Introduction

Surface 'tensile tests', in which tangential loads are applied through surface mounted adhesive pads, have been recognised as viable methods for assessment of mechanical properties of soft materials and

* Corresponding author.
E-mail address: x.j.ren@livjm.ac.uk (X.J. Ren).

0020-7683/$ - see front matter © 2005 Elsevier Ltd. All rights reserved.
doi:10.1016/j.ijsolstr.2005.07.013

particularly in the bioengineering field (Wijn, 1980; Serup and Jemec, 1995; Piérard, 1999; Vescovo et al., 2002; Ren et al., 2003). A common testing configuration (Fig. 1a) consists of two adhesive tapes; one is uniaxially loaded while the other one is static. This testing method is non-destructive, which does not require a pre-cut specimen as in conventional tensile tests. It can also assess directional properties of an anisotropic medium; this makes it more attractive than the other more common loading mode (e.g. indentation) in certain situations (e.g. in vivo skin testing). Due to its complex configuration, the mechanics of the materials under such a loading mode is much more complicated than in conventional tensile tests, in which the material behaviour can be described by a simple stress–strain relationship. It is therefore essential to characterise the displacement–strain patterns in this loading configuration and to investigate the possible effect of the dimensional parameters. Due to the complexity of the strain and stress condition in such surface tests, the material properties have not, so far, been determined by this approach. It can only be used to study comparative materials' behaviour with no direct reference to the real material property. This has made the interpretation and comparison of results from different sources very difficult. A validated method to extract the material properties will greatly enhance its further application in many

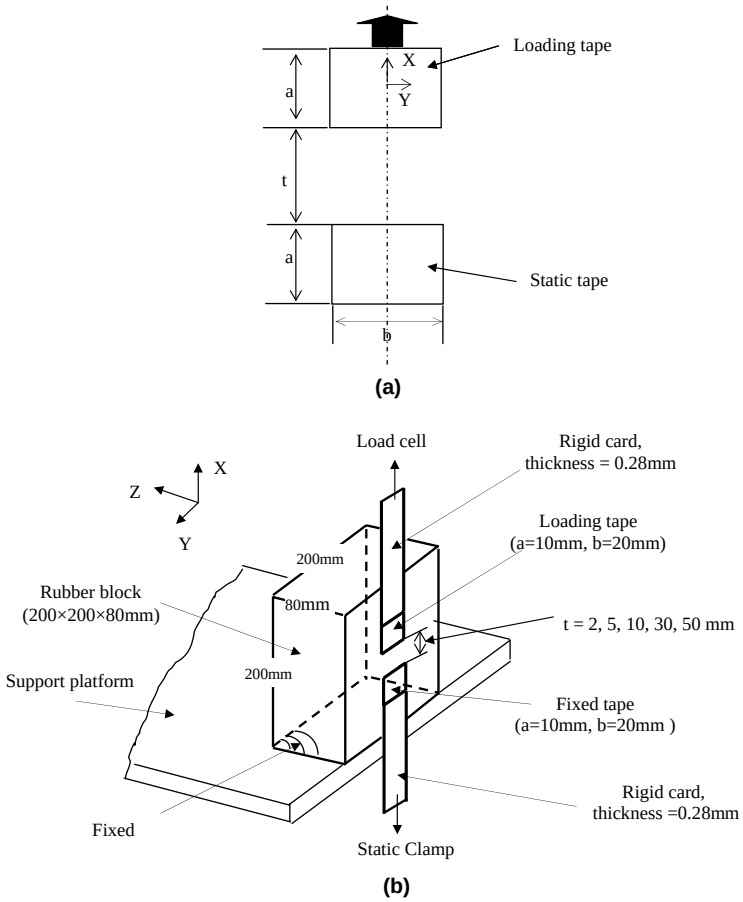

Fig. 1. Schematic to show the surface tensile test and the set-up of the experimental work. (a) Surface tensile test and the dimensional parameters, where x, y, z are the coordinates; b, width of the loaded area; a, length of the loaded area; t, tape separation. (b) Schematic to show the set-up of the experimental work (unit mm).

fields. Analytical works (Ren et al., 2005) on a simpler case (i.e. with one tape only) indicated that material properties may be determined from the load displacement data acquired from different test geometries.

Imaging techniques are very suitable candidates in studying the mechanical behaviour of materials. Smith et al. (1999) successfully used surface displacement analysis software (SDA, Instron Corp., USA) to investigate the displacement and strain of several foams under indentation. Petras and Sutcliffe (1999), using similar software, studied the deformation of sandwich beams. Zhang et al. (2002) used digital correlation to evaluate the mechanical behaviour of arterial tissue in vitro. One advantage of these non-contact methods lies in that there is no change in stiffness resulting from the presence of a sensor. These image analysis methods coupled with finite element modelling are useful tools for study of the mechanics of materials.

In this paper, the mechanics of surface tensile testing are jointly investigated by experimental measurements and numerical simulation using silicone rubber as a model material. The slope of the applied shear stress and displacement data is used to describe the materials behaviour, and the effects of dimensional parameters (mainly the separations between adhesive tapes) were investigated. The displacement–strain patterns were measured using SDA, which showed consistent results with the FE modelling. The effect of loading geometry on the load–displacement relationship were predicted and discussed. Based on the results, a combined experimental–numerical approach to inversely extract material properties using multiple tests with different length scales is proposed and validated using a model material.

2. Methods and materials

2.1. Experimental

Blocks of silicone rubber (Dow Corning, 3-3615) with base and catalyst in a 1:1 ratio were made by casting into square specimens of $200 \times 200 \times 80$ mm. The samples were de-gassed in vacuum after mixing and then cured at 70 °C for 1 h. The Young's Modulus (E) and Poisson's ratio (v) for the material were measured in standard quasi-static tensile tests were found to be 0.13 ± 0.06 MPa and 0.49 ± 0.05, respectively. The tests were carried out on a 10 kN screw-driven universal testing machine (Shimadzu AGS-D). The sample size was $10 \times 5 \times 100$ mm and the loading rate was 5 mm/min. The Poisson's ratio was measured using a videoextensometer simultaneously tracking the markers on the specimen surface and the edge of the specimen during the tensile test. Details of the procedure can be found in (Smith et al., 1999). The material was found to be isotropic and the stress–strain curve is linear within the strain range of this work.

The tangential loading tests were carried out on the same tensile test machine (Shimadzu AGS-D) fitted with a 50 N load cell. As shown schematically in Fig. 1b, the samples were placed on a rigid platform; the bottom face of the specimen was fixed to the platform using adhesives to prevent it moving. A tangential load was applied to the facing vertical surface via one rectangular double-sided adhesive tape (3M Health Care Ltd, UK) with a thickness of 0.15 ± 0.01 mm and stiffness of $\sim$1.1 GPa). A second static tape was placed near to and in line with the loading tape. Typical contact dimensions of the tapes ($a \times b$) were 20×10 mm while the tape separation (t) was varied from 5 to 30 mm in the tests. The rubber block had a cross-section of 200×200 mm and a thickness of 80 mm. The loading tape and static tape were positioned symmetric to the horizontal centreline of the rubber block, and the distance between the outer edges of the tapes and the ends of the rubber block varied from 88.5 to 50 mm depending on the tape separation. The back of the loading and static tapes were adhered to lengths of card ($E \sim 2$ GPa, thickness $= 0.28 \pm 0.01$ mm) themselves clamped to the load cell and machine base, respectively. Because the card has a small flexural stiffness in this configuration the load normal to the sample surface was considered to be zero.

The loading speed was 8.33×10^{-5} m/s (5 mm/min) for all the tests, up to a maximum displacement of 0.5 mm in a linear ramp. No slipping of the adhesive tape was observed within this test range. Two types of measurements were taken on consecutive test runs; the first was data on the displacement of the lower edge of the adhesive tape and the second was on the displacement field of the sample surface between and around the loading tape. Both sets of data were compared with the FE simulations. The displacements of the edges of the adhesive tapes were measured using an edge following strain measurement system (Videoextensometer, Messphysik GmbH, Austria). This requires a CCD camera mounted normal to the sample surface connected to a PC running proprietary software. Data was written to file for post-test analysis.

A second system—Surface Displacement Analysis Software (SDA, Instron Corp., USA) was used to measure the displacement fields generated around the tapes (later shown in Fig. 5). Similar software based systems have been described previously (Smith et al., 1999; Petras and Sutcliffe, 1999). The process involved capturing a series of images of the surface during loading. The SDA software calculates the displacements of a number of 'cells' within a designated 'area of interest' (AOI) using a cellular correlation algorithm to determine the displacement of the centre of each cell in the AOI between a reference frame (normally the starting frame) and a second later frame (normally the end of the test). A map of displacements for each cell within the AOI is generated.

2.2. FE models

The test configuration was modelled by finite element analysis. Due to plane symmetry, half of the sample and tangential loading was modelled (ABAQUS 6.2) as shown in Fig. 2. The dimension of the model is $200 \times 200 \times 80$ mm with a scale of 1:1 to the real sample. The Young's modulus used was 0.134 MPa and a Poisson's ratio of 0.49.

The model was meshed with solid eight noded elements (C3D8) assuming elastic material behaviour. All the nodes on the mid-plane were constrained to simulate the symmetry; the end face was constrained to simulate the boundary condition with the supporting platform. The tape was modelled as a rigid body since it is much stiffer than the specimen. A concentrated force was applied to the loading tape representing the pulling load (F), while the static tape was fixed, i.e. no movement in X and Y directions. A convergence study showed that approximately a mesh of $55 \times 30 \times 15$ elements, for the length, width and through thickness, respectively, were required, with a finer mesh underneath and around the loaded area to increase accuracy. Care was taken to ensure the aspect ratio of the element did not extend the guideline value of 1/5. The largest differences in the displacement of the loaded areas were within 5% of a model with twice the mesh density, thus the mesh density was shown to be sufficient.

3. Results and discussion

3.1. Applied shear stress–displacement relationships

The mean applied shear stress (q_0) could be determined by dividing the total pulling force (F) by the adhered area, i.e.

$$q_0 = \frac{F}{a \times b} \tag{1}$$

Typical experimental and FE results are shown in Fig. 3 for various values of tape separation, t. In all of the cases, the relationship between the applied tangential shear stress and the displacement of the tape, from the FE simulation, showed good agreement with the experimental results. All of the test data are approximately linear. Clearly, the slope of these data represents the resistance of the material. The decrease of this slope

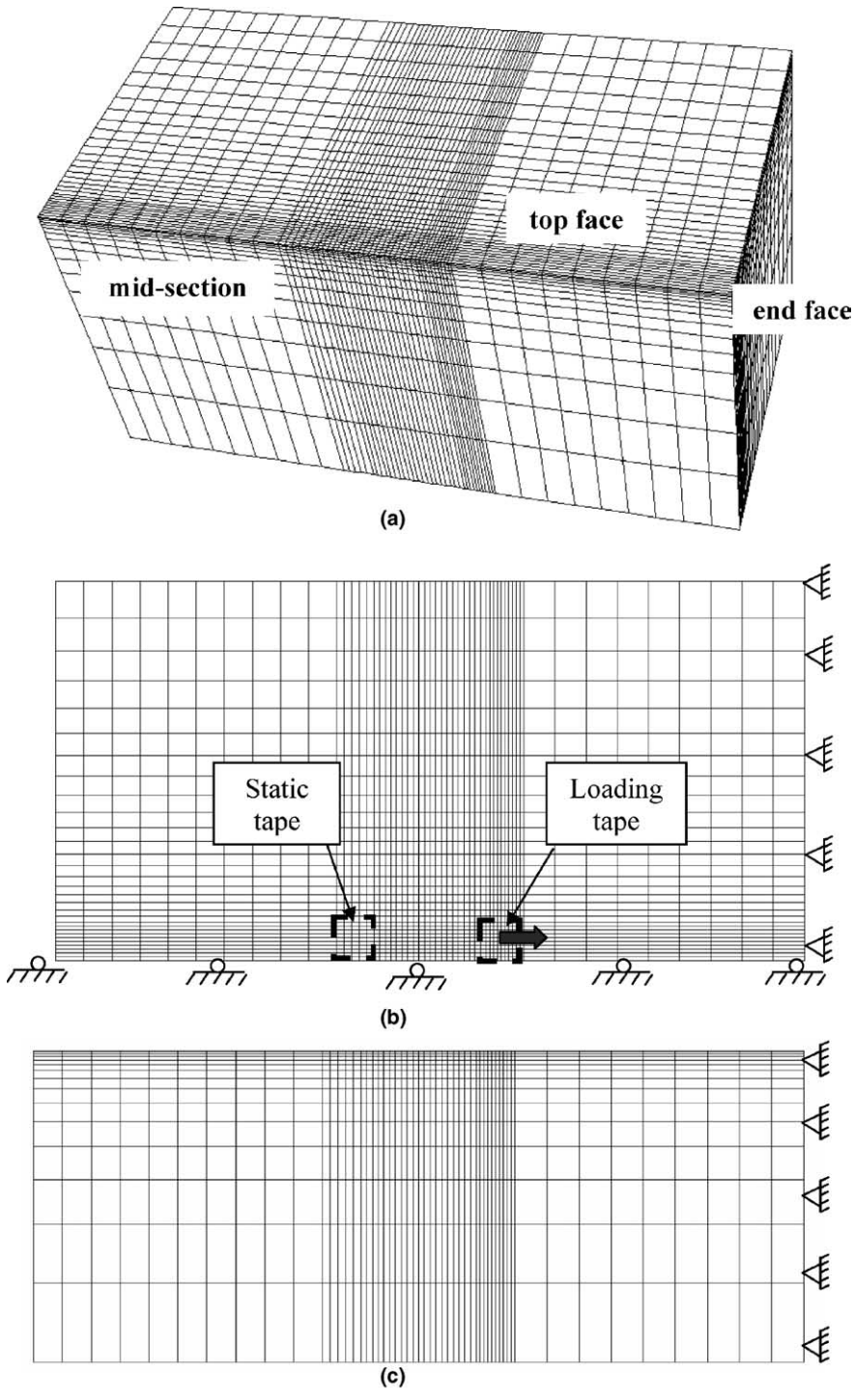

Fig. 2. The FE model: (a) FE model in 3-d, (b) mesh of the top face, (c) mesh of mid-section though the thickness.

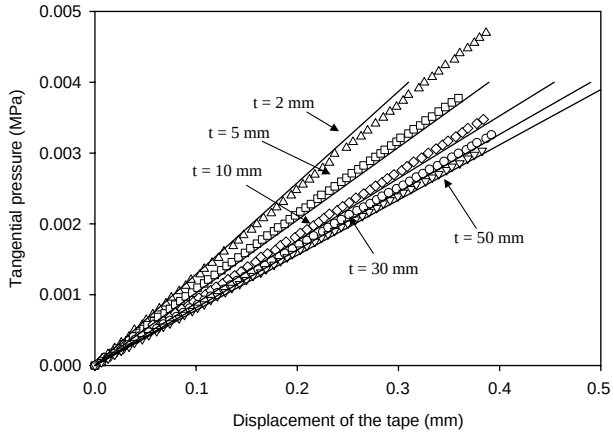

Fig. 3. Typical results of applied shear stress vs. displacement of the tape from the experimental tests (symbols) and FE simulation (solid line) ($a = 10$ mm, $b = 20$ mm, tape separation $t = 2$, 5, 10, 30, 50 mm).

might, at first thought, be associated with both an increase of tape separation and a decrease of the distance of the tapes from the edges of rubber block. To guard against this second effect the shortest distance between the tapes and the edge of the specimen was limited to approximately three times that of the contact length.

Fig. 4 summarises the slope of the applied shear stress and displacement data from experimental tests and FE simulation for various loading dimensions. The x-axis is the ratio of tape separation and adhered length (t/a). For all of the testing dimensions, the experimental and FE results are in good agreement, supporting the validity of the FE model. The slight deviation of the model predictions away from the experimental data (maximum 10%) is probably due to the error in some testing conditions, e.g. incomplete contact between tape and sample surface, etc.

As shown in the Fig. 4, the slope of the applied shear stress and displacement data decreased as the tape separations increased. The decrease was clearly more pronounced for shorter tape separations (i.e. shorter than one tape length). When the tape separation was over three times the tape length, the change became

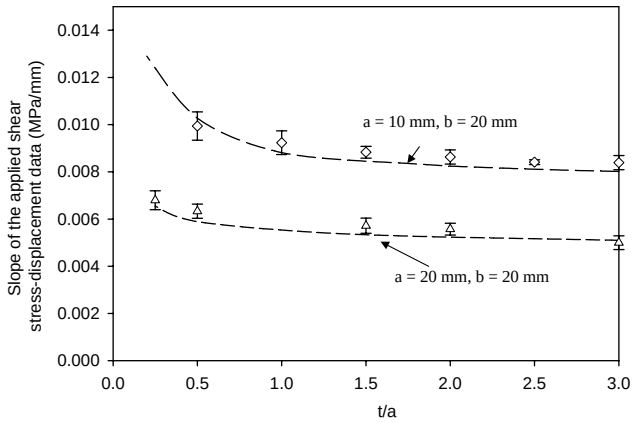

Fig. 4. Effect of tape separation on the slope of the applied shear stress–displacement data from the experimental tests (symbols) and FE simulation (line). The x-axis (tape separation) is normalised against the length of the tape.

very small. The difference between the slope for tape separation of 30 and 50 mm is less than 5% for all the data. This shows that the scale of the effect is principally associated with the ratio of the tape separation and the tape length. When the tape separation is over three times the tape length, its effect becomes very limited and can be ignored.

3.2. Displacement and strain distribution

The pattern of deformation on the surface of the sample between the loading tape and static tape was measured using the SDA software. Fig. 5 is a typical SDA image showing the surface deformation field in the loading direction (U_x). The main area of interest (AOI) was placed between the two tapes. Each cell in the image has a centre point and the vectors represent the displacement of these centre points. The scale of the line is an indicator of the magnitude of surface displacement, which has been magnified by 20 for clarity. The vectors represent the displacement between the final frame and the initial frame, with an applied tape displacement of about 0.5 mm.

Fig. 6 shows the measured and FE model predicted displacement field by plotting the corresponding field in the same scaling. The displacement field between the two tapes (AOI in Fig. 5) agreed well with the FE simulation results. The waviness of the contours in the SDA image is mainly due to experimental noise rather than reflecting real material behaviour. Fig. 7 plots the displacement data along the central axis in the loading direction for various tape separations with a fixed tape dimension (i.e. $a = 10$ mm, $b = 20$ mm). The SDA data (symbols in Fig. 7) was consistent with the prediction of the FE simulation (lines in Fig. 7). In general, results in Figs. 5–7 shows that the surface displacement field in a surface tensile test is obviously not uniform. This is significantly different from conventional tensile tests, in which the main displacement field is uniform and linear (except near the grips) for an isotropic material under uniaxial tension.

In a conventional tensile test, the Poisson's ratio of the material could be determined using the ratio of the lateral and the axial deformation of the materials. Fig. 8 plots a typical surface distribution of the lateral displacement (U_y) between the tapes from FE simulation. The displacement value is much lower than the

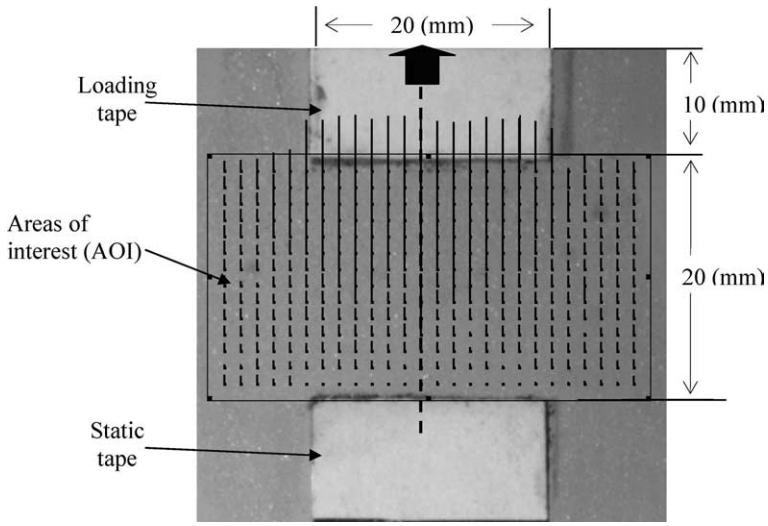

Fig. 5. Typical displacement field calculated by the SDA software, the data in the area of interest (AOI) were later mapped in Fig. 6 and the data along the dotted line were referred to in Fig. 7. The vectors' magnitude is magnified by 20.

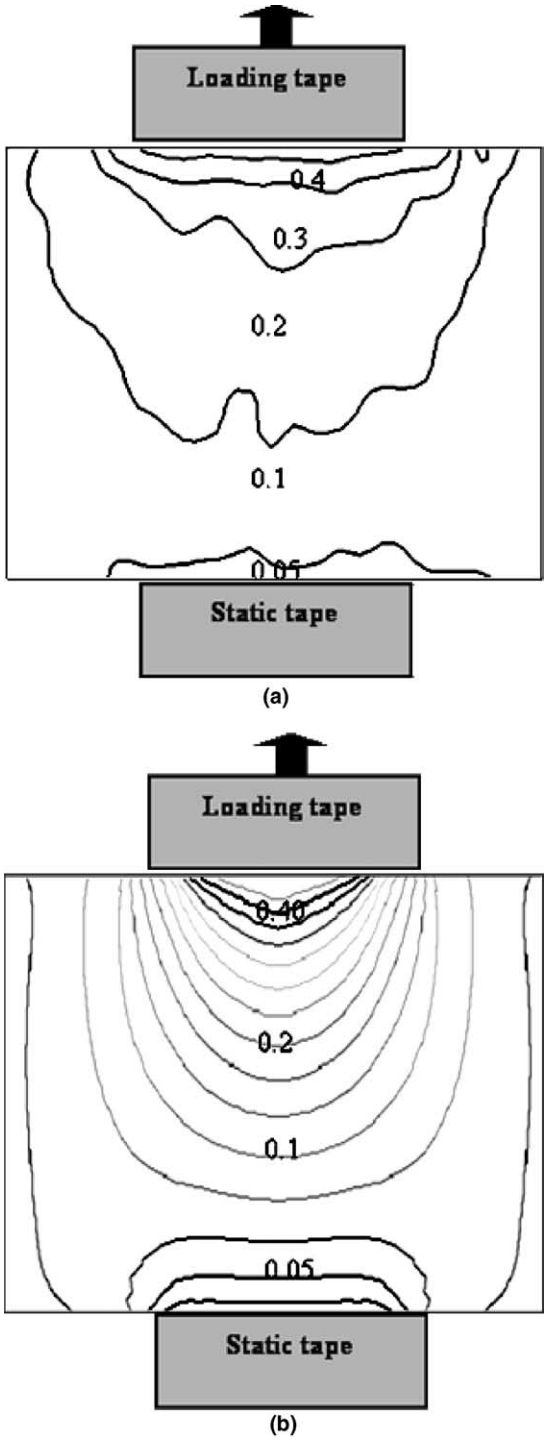

Fig. 6. Comparison of the displacement fields between the tapes (AOI in Fig. 5) produced by SDA (a) and FE simulation (b). All contour values are in mm; the scaling in plot (a) and (b) is the same.

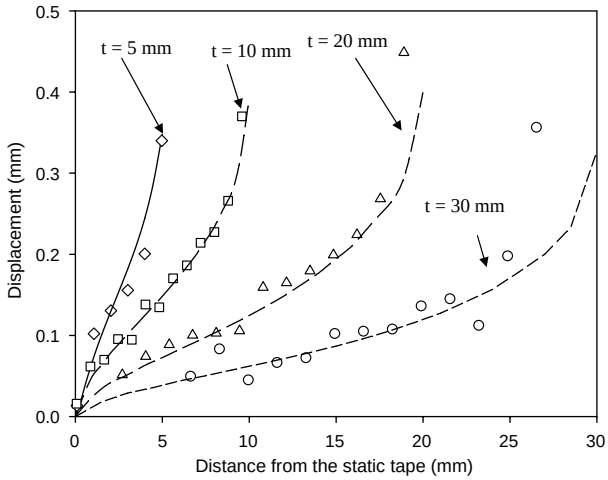

Fig. 7. Displacement data along the loading axis measured by SDA (symbol) and FE (line) for different tape separations ($t = 5$, 10, 20, 30 mm) ($a = 10$ mm, $b = 20$ mm).

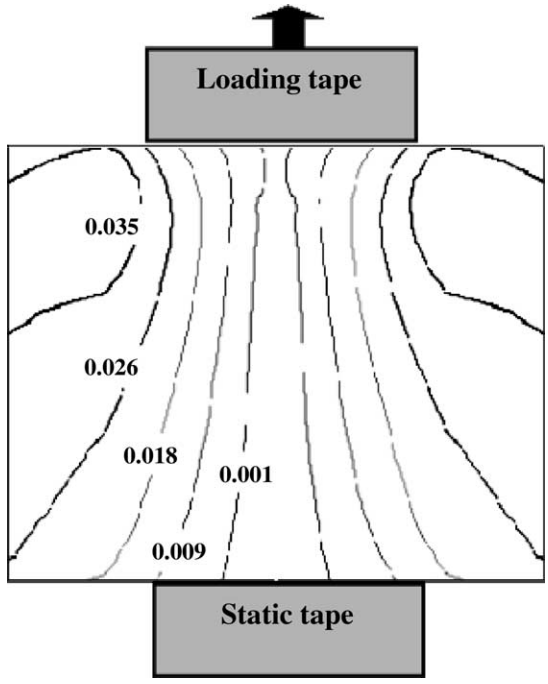

Fig. 8. Typical lateral displacement (U_y in mm) field between the tapes produced by FE simulation ($a = 10$ mm, $b = 20$ mm, $t = 20$ mm).

displacement in the loading direction. This small deformation is out of the measurement limit of the SDA in this work and no consistent results were observed, therefore no experimental result is presented. As shown in Fig. 8, the field is symmetric along the centreline of the tapes but the displacement field is not uniform in the lateral direction. The maximum displacement was located near the corner of the loading tape. This

non-uniform lateral displacement field was also observed in FE models of other testing dimensions including models of infinitely large samples. This is another significant difference between surface tensile and conventional tensile tests, in which the lateral strain displacement field is uniform and the lateral strain can be readily measured to calculate the Poisson's ratio under uniaxial tension. FE simulation also shows that the out of plane deformation is much lower than the in plane deformation (result not shown), which suggests that the image analysis method is suitable for the task. For most of the image displacement analysis programs, both the surface displacement and the strain were measured ignoring the out of plane deformation. The out-of-plane deformation must be significantly lower than the in plane deformation for the technique to be applicable (Zhang et al., 2002).

Fig. 9 shows typical strain data along the centrelines at the loading direction, together with FE results for various tape separations. As shown by the curves, the strain distribution along the centreline produced by the SDA and FE agreed well. It is also shown that the strain field between the tapes is not uniform and not symmetric to the centreline between the tapes. The surface strain is higher near the loading tape and lower toward the static tape. This suggests that the surface strain should not be simply calculated by dividing the tape displacement by the tape separation. In addition, the material effectively involved in the deformation is not clearly defined. Therefore, the behaviour of material is best represented using the applied shear stress–displacement relationship rather than the stress–strain relationship.

3.3. Material properties prediction

As shown in Figs. 7–9, the applied shear stress–displacement data and strain distribution varied with tape separations, which indicate different stress–strain states. This phenomenon can be used to extract the material properties by reproducing the experimental data via finite element modelling of tests with different length scales. This was assessed using the model materials, which is a simple case with two material properties, i.e. E and v. So even though direct measurements of lateral deformation were not available both E and v can be determined from different sets of longitudinal data.

Fig. 10 is a flow chart showing the proposed approach used to extract the material properties of the rubber block used in this work with tapes of adhered area 20×10 mm and three tape separations ($t = 5$, 10 and 20 mm). In the initial stage, one test result (in this case, tape separation, $t = 10$ mm) is used to screen the

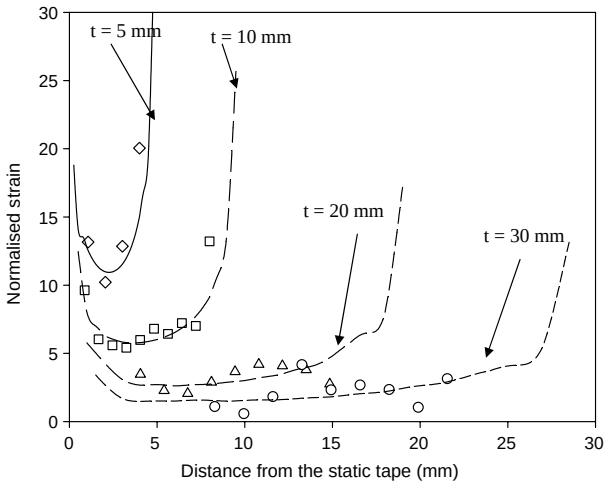

Fig. 9. Strain data (ε_x) along the loading axis measured by SDA (symbol) and FE (line) for different tape separations ($t = 5$, 10, 20, 30 mm) ($a = 10$ mm, $b = 20$ mm).

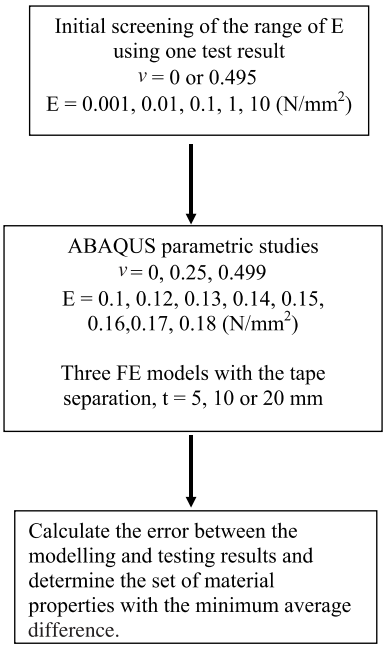

Fig. 10. Overview of the mixed experimental and parametric modelling approach to extract the material properties.

Young's modulus values over a wide range (0.001–10 MPa). For most materials, Poisson's ratio is known to be between 0 and 0.5, unless the structure of the material implies the possibility of a negative Poisson's ratio (Lakes, 1987). Preliminary modelling showed that the shear stress–displacement data continuously varied with the Poisson's ratio; therefore these two values (i.e. 0 and 0.5) could be used to determine the higher and lower bounds of the Young's modulus. Fig. 11 shows the shear stress–displacement data *vs.* Young's modulus with a 10 mm tape separation (in log scales). The horizontal lines represent the testing result

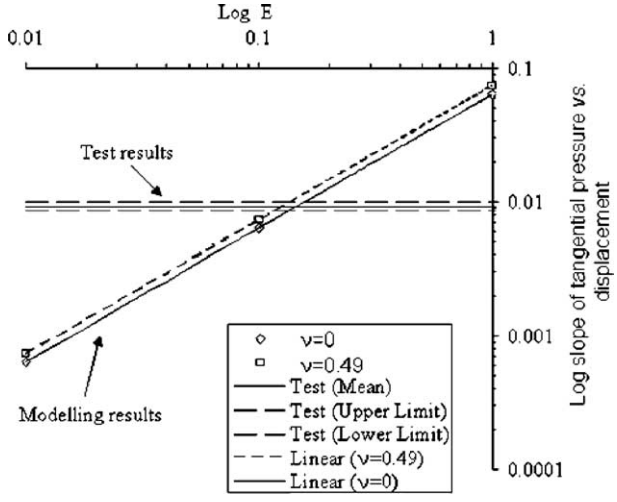

Fig. 11. Initial screening of the range of the Young's modulus (in log scales) ($a = 10$ mm, $b = 20$ mm, $t = 10$ mm).

and the upper and lower error limits. The intersection point between the modelling and testing results were used to define the range of the Young's modulus. The Young's modulus is found to be between 0.11 and 0.16 MPa, which represents a 60% range.

As listed in Fig. 10, in the second stage, parametric studies were performed to close down the range of the material properties. In the parametric studies, the Young's modulus was varied from 0.1 to 0.18 MPa with an increment of 0.01 which gives the predicted Young's modulus an accuracy about 10%. Three Poisson's ratio values used were 0, 0.25, and 0.499. Three FE models with the tape separations of 5, 10 or 20 mm were used in the parametric studies.

The predicted shear stress–displacement results for each combination of material properties (i.e. E and v) were compared to the testing result for the corresponding dimensional condition. The average between the modelling (with one combination of E and v) and testing results was calculated using Eq. (2)

$$S(E,v) = \frac{\sum_{i=1}^{n} \frac{X(E,v) - \overline{X_i}}{\overline{X_i}}}{n} \tag{2}$$

where $S(E,v)$ is the average error between the FE results (3 models) for a set of material properties and the testing results; $X(E,v)$ is the FE modelling results using a set of material properties (E,v); n is number of testing conditions, $n = 3$ representing the three tape separations; $\overline{X}$ is the experimental data.

Fig. 12 summarises the S values for all the material properties sets used in the parametric studies. As shown in the figure, when the Young's modulus is 0.13–0.14 MPa with a Poisson's ratio 0.499, S is the lowest; while the results with other material properties are higher. This suggests that these are the level of the material properties. The predicted result showed very good agreement with the real material properties (i.e. $E = 0.134$ N/mm^2, $v = 0.49$) with an error within 10%. As shown in Fig. 12, the effect of Young's modulus is much more significant than the Poisson's ratio. There is little difference in the curves for Poisson's ratio 0 and 0.25, but the curve for Poisson's ratio 0.49 is clearly different. Normally, the Poisson's ratio is measured from lateral strains due to an imposed axial strain in a standard tensile/compression tests where an isolated specimen is available. However, in surface tensile tests as studied in this work, the volume of the displaced materials is not clearly defined and the displacement field between the tapes is non-uniform as shown in Figs. 7 and 8. These complex displacement fields made it difficult to obtain the strain values to directly calculate the Poisson's ratio analytically. There is no available analytical solution for the testing configuration to directly analyse the effect of materials properties on the force displacement data; however, for a simple

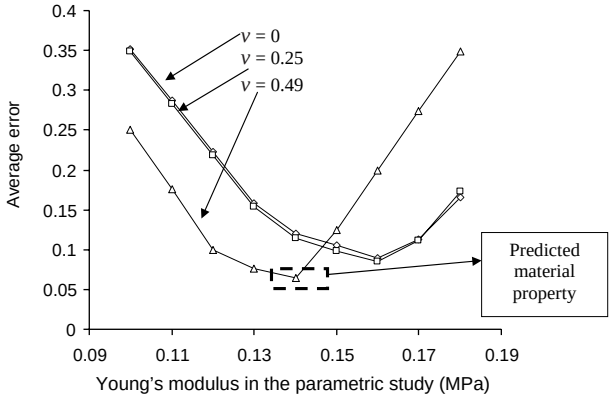

Fig. 12. Average error (S) for different sets of material properties showing the predicted material properties.

case as in a point tangential loading on an elastic half space, the tangential displacement can be calculated using equation (Johnson, 1985):

$$[\overline{u}] = \frac{(1-2v)(1+v)}{2E} Q \tag{3}$$

where Q is a unit concentrated tangential force, which acts tangentially to the surface over an elastic half space; E is the Young's modulus; v is the Poisson's ratio.

So the force displacement relationship can be represented by

$$\frac{Q}{[\overline{u}]} = \frac{2E}{(1-2v)(1+v)} \tag{4}$$

According to Eq. (4), the force displacement relationship will be affected by both the Young's modulus and the Poisson's ratio. In addition, when the tape separation increases, the stress strain state of the materials between the tapes changes, e.g. from a state closer to plain stress ($\sim E$) to a state closer to plain strain ($\sim \frac{E}{(1-v^2)}$). The effect of Poisson's ratio from both sources will contribute to the inverse modelling of the material properties. Sensitivity tests (by comparing the values of $\frac{2E}{(1-2v)(1+v)}$ and $\frac{1}{(1-v^2)}$ of different Poisson's ratios) showed both mechanisms will have more significant effect on the force displacement data at higher Poisson's ratio, which agrees with the trend shown in Fig. 12. It also (results not shown) showed that the effect of Poisson's ratio associated with the former mechanism (Eq. (3)) is much more pronounced than that associated with the change of stress strain state. These demonstrated that the material properties could be estimated using a mixed experimental and numerical method by exploring the effect of Poisson's ratio from these two mechanisms in particular for soft materials in surface tensile tests. Further work will be performed to explore the potential effect of the specimen size to improve the sensitivity of the method.

4. Conclusions

In the present work the deformation and force–displacement relationships in surface tensile tests were investigated jointly by experimental measurements and finite element modelling. Surface displacement analysis (SDA) was successfully used to characterise the deformation fields and showed consistent results with FE simulation using silicone rubber as a model material.

Different from conventional tensile tests, the result of a surface tensile test was highly dependent on the loading dimensions. The slope of the applied shear stress–displacement data is higher when the tapes are closer. When the tape separation is over three times the tape length, its effect becomes insignificant. SDA measurements and FE simulations revealed that both the axial and lateral displacement fields were not uniform and the displacement and strain in the loading direction along the centreline is non-linear. Using this different stress–strain state for different tape separations, a combined experimental–numerical approach to inversely extract material properties using multiple tests with different length scales has been proposed and assessed using the model material.

References

Johnson, K.L., 1985. Contact Mechanics. Cambridge University Press, Cambridge, UK.

Lakes, R.S., 1987. Foam structures with negative Poisson's ratio. Science 235, 1038–1040.

Petras, A., Sutcliffe, M.P.F., 1999. Indentation resistance of sandwich beams. Composite Structure 46 (4), 413–424.

Piérard, G.E., 1999. EEMCO guidance to the in vivo assessment of tensile functional properties of the skin. Skin Pharmacology and Applied Skin Physiology 12, 52–67.

Ren, X.J., Smith, C.W., Evans, K.E., Dooling, P.J., Burgess, A., Wiechers, J.W., Zahlan, N., 2003. The mechanics of skin testing. Society for Experimental Mechanics (SEM) Conference on Mechanics of Biological and Biologically Inspired Materials & Systems, Springfield, Massachusetts, USA.

Ren, X.J., Smith, C.W., Evans, K.E., Dooling, P.J., Burgess, A., Wiechers, J.W., Zahlan, N., 2005. Elastic deformation of materials under tangential loading, in preparation.

Serup, S.J., Jemec, G.B.E., 1995. Handbook of Non-Invasive Methods and the Skin. CRS Press, Florida.

Smith, C.W., Wooton, R.J., Evans, K.E., 1999. Strain dependent densification during indentation in auxetic foams. Cellular Polymer 18, 79–101.

Vescovo, P., Varchon, D., Humbert, P., 2002. In vivo tensile tests on human skin: the extensometers. In: Elsner, P., Berardesca, E., Wilhelm, K.P., Maibach, H.I. (Eds.), Bioengineering of the Skin: Skin Biomechanics. CRC Press LLC, London.

Wijn, P.F.F., 1980. The linear viscoelastic properties of human skin in vivo for small deformations, Ph.D. thesis, Univ Nijmegen.

Zhang, D.S., Eggleton, C.D., Arola, D., 2002. Evaluating the mechanical behaviour of arterial tissue using digital image correlation. Experimental Mechanics 42 (4), 25–35.